MULTISCALE MODEL. SIMUL.
Vol. 12, No. 1, pp. 225–248

TIME CORRELATION FUNCTIONS OF BROWNIAN MOTION AND EVALUATION OF FRICTION COEFFICIENT IN THE NEAR-BROWNIAN-LIMIT REGIME*

CHANGHO KIM† AND GEORGE EM KARNIADAKIS†

Abstract. The exponentially decaying behavior of the momentum-momentum and momentum-force time correlation functions of Brownian motion at large times has been extensively used for the numerical evaluation of the friction coefficient γ from molecular dynamics simulations. We perform *numerical analysis* on these methods and address issues related to the appropriate choice of large time and the rate of convergence of these methods. To this end, we obtain asymptotic expansions of the time correlation functions with respect to the *reduced* mass μ of the Brownian particle. For two important limit procedures of achieving the Brownian limit, certain forms of the asymptotic expansion of the Mori memory function $K(t)$ are introduced by physical arguments, and then the asymptotic expansions of the time correlation functions are expressed in terms of the limit of $K(t)$, i.e., $K_0(t) = \lim_{\mu\to\infty} K(t)$, and the next-order correction term $K_1(t)$. For the infinite mass limit case, we show that the numerical methods of estimating γ from the exponential decay of the time correlation functions produce $\gamma + O(\mu^{-1})$, where the first-order correction depends on the microscopic nature of $K_0(t)$ (i.e., deviation of $K_0(t)$ from the Dirac delta function $\gamma\delta(t)$) as well as the contribution of $K_1(t)$ (i.e., deviation of $K(t)$ from $K_0(t)$). We also analyze the ratio of the momentum-force correlation function to the momentum-momentum correlation function, which gives *instantaneous* exponential decay rate. For the thermodynamic limit case, we consider the Rayleigh gas system to investigate the finite-volume effect due to the boundary conditions and to demonstrate that the lowest-order terms of the asymptotic expansions may fail to describe some characteristic behavior of the time correlation functions. We perform systematic molecular dynamics simulations of the Rayleigh gas system to confirm the theoretical predictions.

Key words. Brownian motion, memory function, molecular dynamics simulation, Rayleigh gas

AMS subject classifications. 82C31, 70K70, 37M05

DOI. 10.1137/130929916

1. Introduction.

The friction coefficient is one of the essential parameters for simulating transport phenomena in colloidal systems, and estimating it precisely in a systematic manner is important from both theoretical and practical points of view. In addition, as experimental techniques have been improved so that the trajectories of Brownian motion can be observed on shorter time scales than the diffusive time scale of the colloid particles [9, 20], understanding the corresponding phenomena at the molecular level becomes more important.

When a Brownian particle suspended in a fluid has much larger mass than the fluid particles, its velocity satisfies the *phenomenological* Langevin equation [19], where the friction coefficient γ enters as a parameter. The microscopic theory of Brownian motion has addressed the issue of deriving the Langevin equation from first principles (i.e., from the Hamilton's equation or Liouville's equation of the molecular system) and expressing the transport coefficient γ in terms of quantities that can be obtained from the microscopic trajectory of the system, hence computationally from molecular dynamics (MD) simulations.

*Received by the editors July 22, 2013; accepted for publication (in revised form) December 16, 2013; published electronically February 27, 2014. This work was partially supported by the new DOE Center on Mathematics for Mesoscopic Modeling of Materials (CM4) and by the NSF (grant DMS-1216437).
http://www.siam.org/journals/mms/12-1/92991.html
†Division of Applied Mathematics, Brown University, Providence, RI 02906 (george_karniadakis@brown.edu, changho_kim@brown.edu).

One such formula proposed by Kirkwood [12] is given by the Green–Kubo expression, where the friction coefficient is related to the time integral of the force autocorrelation function. However, it has a so-called *plateau* problem that the value of the time integral decays to zero as the upper limit of time integration is increased to infinity. Another formula, which has a similar form but does not decay, has been obtained by various techniques [17, 29, 32]; γ is given as the time integral of the force autocorrelation function of the *reference* system. The latter is defined as the frozen dynamics, where the Brownian particle is assumed to be fixed in space and the fluid particles move under the external potential due to the presence of the Brownian particle. Using the projection operator technique, Mazur and Oppenheim [23] performed a detailed analysis of this formula. They defined a projection operator, which is different from the well-known Mori projection operator [25], and showed that the corresponding memory function has a well-behaved series expansion in powers of the mass ratio of a fluid particle to the Brownian particle, and that γ is obtained from the zeroth-order term. They also showed that the total force autocorrelation function has a negative and slowly decaying tail, which makes the time integral of the Kirkwood formula vanish. Based on Mazur and Oppenheim's analysis, Hynes, Kapral, and Weinberg [10] performed a similar analysis on the generalized Langevin equation derived by Mori [25] to show that the Mori memory function also has a slowly decaying tail, but its contribution to the time integral is so negligible in the Brownian limit that the Langevin equation can be derived from the generalized Langevin equation.

Significant progress on understanding the finite-size effect, which is important in MD simulation studies, was made by Español and Zúñiga [5]. They showed that for a Brownian particle suspended in a bath consisting of a *finite* number of particles, the reduced mass μ enters in the generalized Langevin equation rather than the actual mass M of the Brownian particle. Then they obtained asymptotic expressions for the time correlation functions of the Brownian particles for large μ and t (see also [18, 26]):

$$\langle \mathbf{P}(0)\cdot\mathbf{P}(t)\rangle \approx \frac{d}{\beta}\,\mu\, e^{-\frac{\gamma}{\mu}t}, \tag{1.1a}$$

$$\gamma(t) = \frac{\beta}{d}\int_0^t \langle \mathbf{F}(0)\cdot\mathbf{F}(u)\rangle \; du = -\frac{\beta}{d}\,\langle \mathbf{P}(0)\cdot\mathbf{F}(t)\rangle \approx \gamma\, e^{-\frac{\gamma}{\mu}t}, \tag{1.1b}$$

where $\mathbf{P}$ is the momentum of the Brownian particle and $\mathbf{F}$ is the force on the Brownian particle by the fluid (for detailed definitions of other symbols, see section 2.1). Hence, γ can be estimated from the exponential decay rate of $\langle \mathbf{P}(0)\cdot\mathbf{P}(t)\rangle$ and, alternatively, $\langle \mathbf{P}(0)\cdot\mathbf{F}(t)\rangle$ or the time integral of $\langle \mathbf{F}(0)\cdot\mathbf{F}(t)\rangle$ can be used to determine γ by its extrapolated value at $t = 0$ or by its exponential decay rate. Español and Zúñiga also pointed out that in Mazur and Oppenheim's work [23], the thermodynamic limit $N \to \infty$, where N is the number of the bath particles, was implicitly assumed when the infinite mass limit $M \to \infty$ was taken, and hence the Brownian limit is achieved as $\mu \to \infty$. From the hydrodynamic point of view, the density ratio of the Brownian particle and the surrounding fluid is also an important parameter [7]. If the ratio is comparable to unity, the motion of the Brownian particle is affected by the long-lived vortices in the fluid, which were developed by its movement in previous times. This hydrodynamic memory explains that the velocity autocorrelation function of the Brownian particle has a long-time tail of the form $t^{-3/2}$ [8]. For an incompressible fluid, the hydrodynamic Brownian motion is described by the generalized Langevin equation with the Boussinesq–Basset force [21]. The effect of compressibility has been investigated to explain the initial rapid change of the velocity autocorrelation function [33]. Since these hydrodynamic effects become negligible as $\mu \to \infty$, we do not further investigate them in the paper.

Numerous MD studies have been performed on the single Brownian particle system from various points of view, and we only mention herein recent work which is relevant to our present work. Through large-size MD simulations, the time-dependent friction coefficient $\gamma(t)$, defined as the time integral of the total force autocorrelation function (see (1.1b)) has been investigated to determine the friction coefficient γ [18, 26]. The Mori memory function of Brownian motion has been calculated from MD simulations and investigated for various physical parameters in [14, 30]. The convergence of the Mori memory function under the Brownian limit has also been observed [11, 15]. Using the linear response theory and performing nonequilibrium MD simulations, it has been shown that the aforementioned finite-size effect is due to the finite *mass* of the bath rather than the finite *volume* of the bath [28], and an alternative method of estimating γ from a finite system has been proposed [27]. An ad hoc correction of finite-volume effect has also been attempted [31].

The Rayleigh gas model, which additionally assumes no interaction between bath particles (i.e., a Brownian particle in an ideal gas), has provided plenty of insight into Brownian motion. Owing to the noninteracting bath assumption, the system becomes analytically more manageable so that some exact and explicit results are available. The explicit expression for the friction coefficient has been obtained under the assumption of elastic collisions by various techniques [4, 6, 22, 24], and the convergence of the motion of the Brownian particle to the Ornstein–Uhlenbeck process has been proved [3]. Recently, a corresponding proof for a continuous interaction potential case has been provided [16]. Another favorable feature of the Rayleigh gas model is that an infinite bath is naturally introduced, and results without any finite-size effect can be obtained. The force autocorrelation function of the infinite reference system, the time integral of which gives the friction coefficient, has been investigated for various types of interaction potentials [11]. This quantity was accurately calculated from numerical integration of one-particle trajectories of a bath particle and then compared with MD simulation results.

In this paper, we develop a theory that enables precise and systematic analysis of MD simulation results of the single Brownian system in the near-Brownian-limit regime. More specifically, we obtain asymptotic expansions of the time correlation functions $\langle \mathbf{P}(0) \cdot \mathbf{P}(t) \rangle$, $\langle \mathbf{P}(0) \cdot \mathbf{F}(t) \rangle$, and $\langle \mathbf{F}(0) \cdot \mathbf{F}(t) \rangle$ with respect to μ. Noting that the asymptotic behaviors in (1.1) for large t and μ have been extensively used to determine the value of γ but very little has been theoretically investigated about the criteria for choosing the large values of t and μ and the convergence rate of the evaluated values to γ, we tackle these issues using asymptotic expansions of the time correlation functions. Although we can retrieve (1.1) from the asymptotic expansions for large t, it is noted that t is not an asymptotic parameter in these asymptotic expansions, and hence we can use them for *short* and *intermediate* times as well. Unless explicitly indicated as t-asymptotic or (t, μ)-asymptotic, we use the term *asymptotic* as μ-asymptotic in the rest of the paper. To derive the asymptotic expansions of the time correlation functions, we use the asymptotic expansion of the Mori memory function $K(t)$. Since the form of the asymptotic expansion of $K(t)$ depends on the limit procedure of achieving the Brownian limit, we consider two important cases. For the first case, where the infinite mass limit $M \to \infty$ is taken under the assumption that the thermodynamic limit $N \to \infty$ has been already achieved (i.e., a finite-mass

Brownian particle in an infinite bath), we perform detailed analysis on the numerical methods of determining γ based on (1.1). In addition, we analyze the ratio of $\langle \mathbf{P}(0) \cdot \mathbf{F}(t) \rangle$ to $\langle \mathbf{P}(0) \cdot \mathbf{P}(t) \rangle$, which gives an *instantaneous* exponential decay rate. For the second case, where an infinite mass is assumed for the Brownian particle and the thermodynamic limit is taken (i.e., frozen dynamics in a finite bath), a Rayleigh gas is considered and the finite-volume effect due to the boundary conditions is investigated. To demonstrate the validity of the theory, we perform extensive MD simulations of the Rayleigh gas for the two limit cases.

The rest of the paper is organized as follows. We derive the asymptotic expansions of the time correlation functions in section 2. We present the analysis on the numerical methods of evaluating the friction coefficient in section 3. The MD simulation results are given in section 4. We provide a summary with some discussion in section 5.

2. Asymptotic expansions of time correlation functions.

2.1. System. We follow the standard setting of the system for microscopic description of a single Brownian particle [10, 23]. A Brownian particle of mass M is suspended in a bath of volume V in a d-dimensional space ($d = 2$ or 3). The bath consists of N bath particles of mass m. The inverse temperature of the system is denoted by $\beta = (k_{\mathrm{B}}T)^{-1}$. Although assuming a specific form of interaction potentials between the Brownian particle and a bath particle and between bath particles is not essential, we introduce the usual assumption that they are functions of interparticle distance and are short-ranged. The latter is introduced because the interaction between the Brownian particle and a bath particle is assumed to be instantaneous on the Brownian time scale.

We denote the momentum of the Brownian particle by $\mathbf{P}$ and the force on the Brownian particle by $\mathbf{F}$. We note the following relation, which was derived by Español and Zúñiga [5]:

$$\langle \mathbf{P} \cdot \mathbf{P} \rangle = \frac{d}{\beta}\mu, \tag{2.1}$$

where the brackets denote the equilibrium average and the reduced mass μ is defined as

$$\mu = \frac{MNm}{M + Nm}. \tag{2.2}$$

In this paper, the Brownian limit is defined as $\mu \to \infty$, which is equivalent to achieving *both* the infinite mass limit $M \to \infty$ and the thermodynamic limit $N \to \infty$. When increasing the number of bath particles, we also increase the volume of the system so that the number density N/V stays constant. Other physical conditions such as the temperature and parameters of the interaction potentials, including the size of the Brownian particle, do not change when these limits are achieved.

As mentioned in the introduction, we are interested in the time correlation functions $\langle \mathbf{P}(0) \cdot \mathbf{P}(t) \rangle$, $\langle \mathbf{P}(0) \cdot \mathbf{F}(t) \rangle$, and $\langle \mathbf{F}(0) \cdot \mathbf{F}(t) \rangle$ in the near-Brownian-limit regime $\mu \gg m$ (or, equivalently, $M \gg m$ and $N \gg 1$).

2.2. Generalized Langevin equation. The starting point of the theory is the following generalized Langevin equation [5, 25]:

$$\dot{\mathbf{P}}(t) = -\frac{1}{\mu} \int_0^t K(t-u)\mathbf{P}(u)\, du + \mathbf{F}^{+}(t), \tag{2.3}$$

where $K(t)$ is the Mori memory function and $\mathbf{F}^+$ is the fluctuating force satisfying

$$\left\langle \mathbf{F}^+(t) \right\rangle = 0, \quad \left\langle \mathbf{P}(0) \cdot \mathbf{F}^+(t) \right\rangle = 0, \quad \mathbf{F}^+(0) = \mathbf{F}(0). \tag{2.4}$$

It is important to realize that this equation is *exact* although the explicit form of $K(t)$ is unknown. The fluctuation-dissipation relation is given as

$$K(t) = \frac{\beta}{d} \left\langle \mathbf{F}^+(0) \cdot \mathbf{F}^+(t) \right\rangle . \tag{2.5}$$

As mentioned in the introduction, it is noted that because of (2.1), the factor in (2.3) is μ^{-1} rather than M^{-1}.

We denote the momentum autocorrelation function as

$$C(t) = \langle \mathbf{P}(0) \cdot \mathbf{P}(t) \rangle . \tag{2.6}$$

Then the other time correlation functions are given as time derivatives of $C(t)$:

$$\langle \mathbf{P}(0) \cdot \mathbf{F}(t) \rangle = \dot{C}(t), \quad \langle \mathbf{F}(0) \cdot \mathbf{F}(t) \rangle = -\ddot{C}(t). \tag{2.7}$$

From (2.1), (2.3), and (2.4), we obtain a Volterra integrodifferential equation for $C(t)$:

$$\dot{C}(t) = -\frac{1}{\mu} \int_0^t K(t-u) C(u)\, du, \quad C(0) = \frac{d}{\beta}\mu. \tag{2.8}$$

2.3. Solution of (2.8). By using the Laplace transform technique, we solve (2.8) for $C(t)$ (i.e., express $C(t)$ in terms of $K(t)$). We denote the Laplace transform of a function by using tilde notation and use s as the Laplace variable. For example,

$$\tilde{C}(s) = \int_0^\infty C(t) e^{-st} dt. \tag{2.9}$$

From (2.8), we obtain

$$\tilde{C}(s) = \frac{C(0)}{s + \frac{1}{\mu}\tilde{K}(s)} = \frac{C(0)}{s} \sum_{n=0}^{\infty} \left(-\frac{1}{\mu s} \tilde{K}(s) \right)^n , \tag{2.10}$$

where we assumed that the series expansion is well-defined. Then we obtain the following series solution for $C(t)$:

$$C(t) = C(0) \left[1 + \sum_{n=1}^{\infty} \frac{(-1)^n}{\mu^n} \int_0^t G^{*n}(u)\, du \right] , \tag{2.11}$$

where

$$G(t) = \int_0^t K(u)\, du, \tag{2.12}$$

and $G^{*n}(t)$ is the n-fold convolution power of $G(t)$ defined recursively as

$$G^{*1}(t) = G(t), \quad G^{*(n+1)}(t) = (G^{*n} * G)(t) = \int_0^t G^{*n}(t-u) G(u)\, du. \tag{2.13}$$

To obtain (2.11), we used properties such as $\tilde{G}(s) = \tilde{K}(s)/s$ and $\widetilde{G^{*n}}(s) = \left[\tilde{G}(s)\right]^n$.

2.4. $K_0(t)$ and $C_0(t)$. Although we expressed $C(t)$ in terms of $K(t)$ in (2.11), it is noted that the explicit form of $K(t)$ is unknown in practice and, in an MD simulation study, it is obtained by calculating the time correlation functions (i.e., $C(t)$ and its derivatives) and solving (2.8) for $K(t)$ [30] (see also [13]). It is also noted that when the value of N or M varies, both $K(t)$ and $C(t)$ vary. Hence, it appears that there is not much gain from the solution (2.11). However, as observed in several MD simulation studies [11, 14, 30], compared to the change of the overall shape of $C(t)$ and its derivatives for varying μ, that of $K(t)$ is much smoother. In addition, while $C(t)$ does not possess a proper limit under $\mu \to \infty$, $K(t)$ has a well-defined limit, denoted by $K_0(t)$. For the finite value of μ, we express $K(t)$ as follows:

$$K(t) = K_0(t) + \delta K(t). \tag{2.14}$$

Using $K_0(t)$ and the lowest-order term $K_1(t)$ of $\delta K(t)$, we shall obtain an asymptotic expansions of $C(t)$ with respect to μ in section 2.5.

The friction coefficient γ is expressed in terms of $K_0(t)$ as follows. Since both $\langle \mathbf{F}(0) \cdot \mathbf{F}(t) \rangle$ and $\langle \mathbf{F}^+(0) \cdot \mathbf{F}^+(t) \rangle$ converge to the frozen dynamics force autocorrelation function of the reference system [5], we have the following relations using (2.5):

$$K_0(t) = \frac{\beta}{d} \lim_{\mu\to\infty} \left\langle \mathbf{F}^+(0) \cdot \mathbf{F}^+(t) \right\rangle = \frac{\beta}{d} \lim_{\mu\to\infty} \left\langle \mathbf{F}(0) \cdot \mathbf{F}(t) \right\rangle . \tag{2.15}$$

Since γ is given as the time integral of $\lim_{\mu\to\infty} \langle \mathbf{F}(0) \cdot \mathbf{F}(t) \rangle$ [23], we have

$$\gamma = \frac{\beta}{d} \int_0^\infty \lim_{\mu\to\infty} \langle \mathbf{F}(0) \cdot \mathbf{F}(t) \rangle \, dt = \int_0^\infty K_0(t) \, dt. \tag{2.16}$$

Now, using $K_0(t)$, we define $C_0(t)$ as

$$C_0(t) = C(0) \left[1 + \sum_{n=1}^{\infty} \frac{(-1)^n}{\mu^n} \int_0^t G_0^{*n}(u) \, du \right], \tag{2.17}$$

where $G_0(t)$ is correspondingly defined as

$$G_0(t) = \int_0^t K_0(u) \, du. \tag{2.18}$$

It is noted that $C_0(t)$ is the solution of (2.8) if $K(t)$ *would* be replaced by $K_0(t)$. Following the procedure demonstrated in [1] with $\tilde{K}_0(0) = \gamma$ from (2.16), it can be shown that, for large μ and t,

$$C_0(t) \approx C(0) \, e^{-\frac{1}{\mu}\tilde{K}_0(0)t} = \frac{d}{\beta} \, \mu \, e^{-\frac{\gamma}{\mu}t}. \tag{2.19}$$

Hence, the comparison of (1.1a) and (2.19) shows that $C(t)$ and $C_0(t)$ have the same lowest-order asymptotic expressions. Roughly speaking, as $K(t)$ approaches $K_0(t)$ for large μ, $C(t)$ can be approximated by $C_0(t)$. However, in order to make this argument rigorous, we need to take the term $\delta K(t)$ into account and obtain an asymptotic expansion of $C(t)$ for large but finite μ. In section 2.5, we obtain such an expansion, which has $C_0(t)$ as the lowest-order term and higher-order terms of which are given as convolutions of $C_0(t)$ and $\delta K(t)$. In addition, we note that although $C_0(t)$ and $C(t)$ have the same lowest-order asymptotic expressions, their higher-order corrections of the (t, μ)-asymptotic exponential decay behaviors are different due to the contribution of $\delta K(t)$; see sections 3.1 and 3.2.

2.5. Asymptotic expansion of $C(t)$. It is important to realize that the deviation $\delta K(t)$ of $K(t)$ from $K_0(t)$ depends on the limiting procedure of achieving the Brownian limit $\mu \to \infty$ (i.e., how M and N are increased). We shall obtain asymptotic expansions of $C(t)$ and its derivatives for two specific forms of $\delta K(t)$. For each case, we first discuss when the assumed form of $K(t)$ appears and then obtain the asymptotic expansions.

2.5.1. Case A ($\mu \approx M$). Here, we assume that

$$K(t) \approx K_0(t) + \frac{1}{\mu} K_1(t), \tag{2.20}$$

where $K_1(t)$ does not depend on μ. This form of $K(t)$ appears when we take the infinite mass limit $M \to \infty$ assuming the thermodynamic limit $N \to \infty$ is already achieved or assuming the condition $M \ll Nm$. Hence, in this case, μ is approximately equal to M. Hynes, Kapral, and Weinberg [10] considered this case and showed that the Mori memory function is decomposed into two contributions, which they denoted as $i\Omega_{11}(t)$ and $\Delta_{11}(t)$. In particular, $i\Omega_{11}(t)$ is given as the Maxwellian average (with respect to $\mathbf{P}$) of the Mazur–Oppenheim memory function [23], which allows a well-behaved expansion in powers of the mass ratio m/M, whereas $\Delta_{11}(t)$ decays on the slow time scale of the Brownian particle, which does not allow such an expansion. However, it was shown that the magnitude of $\Delta_{11}(t)$ is negligible (i.e., $o(m/M)$). Hence, we have (2.20) with $K_1(t)$ given as the first-order term in the expansion of $i\Omega_{11}(t)$.

By substituting (2.20) into (2.10), we obtain

$$\tilde{C}(s) \approx \frac{C(0)}{s + \frac{1}{\mu}\tilde{K}_0(s)} \sum_{n=0}^{\infty} \left(-\frac{\frac{1}{\mu^2}\tilde{K}_1(s)}{s + \frac{1}{\mu}\tilde{K}_0(s)} \right)^n, \tag{2.21}$$

and, subsequently, by introducing

$$\tilde{C}_0(s) = \frac{C(0)}{s + \frac{1}{\mu}\tilde{K}_0(s)}, \tag{2.22}$$

we obtain

$$\tilde{C}(s) \approx \tilde{C}_0(s) \sum_{n=0}^{\infty} \left(-\frac{1}{C(0)\mu^2} \tilde{K}_1(s)\tilde{C}_0(s) \right)^n. \tag{2.23}$$

Hence, we obtain the following asymptotic expansion of $C(t)$:

$$C(t) \approx C_0(t) + \sum_{n=1}^{\infty} \left(-\frac{1}{C(0)\mu^2} \right)^n K_1^{*n} * C_0^{*(n+1)}(t). \tag{2.24}$$

We note that, contrary to the expansion of $C_0(t)$ (see (2.17)), keeping a finite number of lower terms does not cause divergence as $t \to \infty$ owing to the exponential decay of $C_0(t)$ (for the decay behavior of the lowest-order term $C_0(t)$ and the higher-order terms, see (3.8) and (3.9), respectively). Hence, in practice, we can use the following asymptotic expansion:

$$C(t) \approx C_0(t) - \frac{1}{C(0)\mu^2} \left(K_1 * C_0 * C_0 \right)(t). \tag{2.25}$$

The corresponding asymptotic expansions of the first and second derivatives are given as

$$\dot{C}(t) \approx \dot{C}_0(t) - \frac{1}{\mu^2} K_1 * C_0(t) - \frac{1}{C(0)\mu^2} \left(K_1 * C_0 * \dot{C}_0 \right)(t), \tag{2.26}$$

$$\ddot{C}(t) \approx \ddot{C}_0(t) - \frac{C(0)}{\mu^2} K_1(t) - \frac{1}{\mu^2} K_1 * \dot{C}_0(t) - \frac{1}{C(0)\mu^2} \left(K_1 * C_0 * \ddot{C}_0 \right)(t). \tag{2.27}$$

However, as shown in section 3.2, by including all terms in (2.24), we obtain the correction to the exponential decay rate of $C(t)$ due to $K_1(t)$. Roughly speaking, (2.25) approximates (2.24) under the assumption that the approximation

$$e^{-\frac{\tilde{K}_1(0)}{\mu^2} t} \approx 1 - \frac{\tilde{K}_1(0)}{\mu^2} t \tag{2.28}$$

is valid.

2.5.2. Case B (frozen dynamics of a Rayleigh gas). Here, we consider a *fixed* Brownian particle immersed in a bath with a *finite* number of bath particles. Hence, we achieve the Brownian limit by increasing the number of bath particles (i.e., by taking the thermodynamic limit). To the best of our knowledge, how the Mori memory function of a finite system converges to that of the infinite reference system has not been known in this case. We investigate this problem under the *noninteracting* bath assumption. In other words, we obtain the form of $\delta K(t)$ for the frozen dynamics of the Rayleigh gas in a finite bath. We first obtain the form of the tail appearing in the force autocorrelation function in the finite system and then derive the form of $\delta K(t)$.

In order to make the argument clear, we assume that the volume of the bath is given as $V = L^d$, where L is the side of the bath, and periodic boundary conditions are imposed. In addition, we assume that the interaction between the Brownian particle and a bath particle is purely repulsive. Since the number of bath particles, N, is increased with N/V constant, μ is proportional to L^d. Contrary to the force autocorrelation function $\langle \mathbf{F}(0) \cdot \mathbf{F}(t) \rangle$ of the infinite reference system, which is essentially zero at large times, that of the finite system has a small magnitude at large times. This is attributed to the re-collisions of bath particles to the fixed Brownian particle (in the image cells), which results from the introduction of the boundary conditions.

As derived in the appendix, the force autocorrelation function of the Brownian particle interacting with the gas through elastic collisions has a negative tail of the form $L^{-d} f(t/L)$. Roughly speaking, this is because the time scale of the re-collision is proportional to L, and the probability of the re-collision decays like $\mathrm{O}(L^{d-1})$. We borrow this result for the purely repulsive potential case. Then, by using (2.15), the force autocorrelation function of the finite system is expressed as

$$\langle \mathbf{F}(0) \cdot \mathbf{F}(t) \rangle = \frac{d}{\beta} K_0(t) + \frac{1}{\mu} f\left(\frac{t}{\mu^{1/d}} \right). \tag{2.29}$$

We note that only the contribution of the *first* re-collisions to the *nearest* periodic images (i.e., separated by L) is considered in (2.29). However, the other collisions occur at longer times, and (2.29) is a good enough approximation for our purpose.

To derive the form of $\delta K(t)$, we use the following equation, which is obtained by differentiating (2.8) with respect to t:

$$K(t) = -\frac{\beta}{d} \ddot{C}(t) - \frac{\beta}{d\mu} K * \dot{C}(t). \tag{2.30}$$

Substituting (2.29) into (2.30), we obtain

$$K(t) = K_0(t) + \frac{\beta}{d\mu} f\left(\frac{t}{\mu^{1/d}}\right) - \frac{\beta}{d\mu} K * \dot{C}(t). \tag{2.31}$$

Hence, we obtain $K(t) \approx K_0(t) + \mu^{-1} K_1(t)$, where

$$K_1(t) = -\frac{\beta}{d} K_0 * \dot{C}_0(t) + \frac{\beta}{d} f\left(\frac{t}{\mu^{1/d}}\right). \tag{2.32}$$

We note that $K_1(0) = 0$ and the convolution term initially dominates $K_1(t)$ until the effect of re-collisions becomes significant.

By following the same procedure as in section 2.5.1 and using the Laplace transform of $K(t)$,

$$\tilde{K}(s) = \tilde{K}_0(s) + \frac{1}{\mu} \frac{\tilde{K}_0^2(s)}{s + \frac{1}{\mu}\tilde{K}_0(s)} + \frac{\beta}{d} \frac{1}{\mu^{1-1/d}} \tilde{f}(\mu^{1/d} s), \tag{2.33}$$

we obtain the same form of the asymptotic expansions, (2.25), (2.26), and (2.27) with $K_1(t)$ defined in (2.32).

3. Evaluation of $\boldsymbol{\gamma}$. In this section, we analyze the numerical methods of evaluating γ that make use of the long-time behavior of $C(t)$ or $\dot{C}(t)$. More specifically, we consider the following values:

1. γ_1 obtained from the exponential decay rate of $C(t)$ at large times;
2. γ_2 obtained from the extrapolated value at $t = 0$ from $\dot{C}(t)$ at large times;
3. γ_3 obtained from the exponential decay rate of $\dot{C}(t)$ at large times;
4. γ_4 obtained from the extrapolated value at $t = 0$ from the instantaneous exponential decay rate $-\dot{C}(t)/C(t)$ at large times.

Throughout this section, we consider Case A (i.e., assuming $M \ll Nm$ and the finite-volume effect is not significant). In addition, we introduce some time scales τ_0 and τ_1 on $K_0(t)$ and $K_1(t)$, respectively, so that we assume

$$K_0(t) = 0 \quad \text{for } t > \tau_0, \tag{3.1a}$$

$$K_1(t) = 0 \quad \text{for } t > \tau_1. \tag{3.1b}$$

We note that τ_0 is comparable to or longer than the time duration of a single collision between the Brownian particle and a bath particle. Since $K_0(t)$ and $K_1(t)$ smoothly decay to zero, the assumptions in (3.1) do not hold exactly in practice. For a typical shape of $K_0(t)$ and $K_1(t)$, see Figure 3.

By using the following three parameters, we shall obtain the asymptotic behavior of γ_1, γ_2, γ_3, and γ_4:

$$\gamma \equiv \int_0^{\tau_0} K_0(u)\, du, \quad \alpha \equiv \gamma\tau_0 - \int_0^{\tau_0} G_0(u)\, du, \quad \zeta \equiv \int_0^{\tau_1} K_1(u)\, du. \tag{3.2}$$

While the total effect of $K_0(t)$ and $K_1(t)$ is considered in γ and ζ, respectively, the effect of microscopic structure of $K_0(t)$ (i.e., deviation of $K_0(t)$ from Dirac delta function $\gamma\delta(t)$) is reflected in α.

We first obtain (t, μ)-asymptotic expressions of $C_0(t)$ and $C(t)$ in sections 3.1 and 3.2, respectively, to find estimates for γ_1, γ_2, γ_3, and γ_4. Then, to address the issue of the validity time interval, we analyze lower-order terms with respect to μ, which contribute linear approximations of $C(t)$ and $\dot{C}(t)$ with respect to t in sections 3.3, 3.4, and 3.5.

3.1. (t,μ)-Asymptotic expression of $C_0(t)$. Under the assumption (3.1), we have, for $t > \tau_0$,

$$\int_0^t G_0(u)\,du = \gamma t - \alpha. \tag{3.3}$$

Similarly, after some transient time $n\tau_0$, the time integral $\int_0^t G^{*n}(u)du$ exhibits t-asymptotic behavior and becomes a polynomial of t having degree n. We obtain the two highest-order terms in the polynomial by using the following identity:

$$\int_0^t G_0^{*n}(u)\,du = \int_0^t dt_1\, G_0(t_1) \int_0^{t-t_1} dt_2\, G_0(t_2) \cdots \int_0^{t-\sum_{k=1}^{n-1} t_k} dt_n\, G_0(t_n), \tag{3.4}$$

which can be easily shown by mathematical induction. For large t, by approximating the integrand $G_0(t_1)\ldots G_0(t_n)$ as a constant equal to γ^n over the whole region, we obtain the leading term as $\gamma^n t^n/n!$. To obtain the next highest term, we assume $t > n\tau_0$ and consider the following subregions. In the region satisfying $t_k > \tau_0$ for $k = 1,\ldots,n$ and $\sum_{k=1}^n t_k < t$, the integrand is exactly γ^n, and hence the integration over this region is equal to $\gamma^n(t-n\tau_0)^n/n!$. In the region satisfying $0 < t_1 < \tau_0$, $t_k > \tau_0$ for $k = 2,\ldots,n$ and $\sum_{k=2}^n t_k < t-\tau_0$, the integrand becomes $G_0(t_1)\gamma^{n-1}$, and hence the integration over the region is equal to $\gamma^{n-1}(\gamma\tau_0-\alpha)(t-n\tau_0)^{n-1}/(n-1)!$. Since there are $n-1$ similar subregions and the volume of the remaining region is $o(t^{n-1})$, we obtain

$$\int_0^t G_0^{*n}(u)\,du = \frac{1}{n!}\gamma^n(t-n\tau_0)^n + \frac{n}{(n-1)!}\gamma^{n-1}(\gamma\tau_0-\alpha)(t-n\tau_0)^{n-1} + o(t^{n-1}), \tag{3.5}$$

and, equivalently,

$$\int_0^t G_0^{*n}(u)\,du = \frac{1}{n!}\gamma^n t^n - \frac{n}{(n-1)!}\alpha\gamma^{n-1}t^{n-1} + o(t^{n-1}). \tag{3.6}$$

By substituting (3.6) to (2.17), we have

$$C_0(t) \approx \frac{d}{\beta}\mu \sum_{n=0}^{\infty} \frac{1}{n!}\left(-\frac{\gamma}{\mu}t\right)^n \left[1 + \frac{(n+1)\alpha}{\mu}\right], \tag{3.7}$$

and by using the approximation $(1+\alpha/\mu)^{n+1} \approx 1 + (n+1)\alpha/\mu$ for large μ, we finally obtain

$$C_0(t) \approx \frac{d}{\beta}\mu\left(1+\frac{\alpha}{\mu}\right)\exp\left[-\frac{\gamma}{\mu}\left(1+\frac{\alpha}{\mu}\right)t\right]. \tag{3.8}$$

We note that although we assumed both t and μ are large in the above derivation, it is not clear what the criteria for t and μ are for (3.8) to be valid. Especially, the validity time interval for (3.6), $t > n\tau_0$, depends on n. We revisit this issue in sections 3.3, 3.4, and 3.5.

3.2. (t,μ)-Asymptotic expression of $C(t)$. Using the asymptotic expansion of $C(t)$, (2.24), and the first-order-corrected asymptotic expression of $C_0(t)$, (3.8), we obtain the (t,μ)-asymptotic expression of $C(t)$. We introduce the following rather crude assumptions to estimate the correction terms in (2.24). We assume that $C_0(t)$

is exactly given by (3.8) for all t and $K_1(t)$ is a Dirac delta function, $\zeta\delta(t)$ (i.e., $G_1(t) = \int_0^t K_1(u)du = \zeta$ for all t). Then, we obtain

$$\frac{1}{[C_0(0)]^n} K_1^{*n} * C_0^{*(n+1)}(t) = \frac{1}{n!}\zeta^n t^n C_0(t), \tag{3.9}$$

and by substituting this into (2.24), we finally obtain

$$C(t) \approx \frac{d}{\beta}\mu\left(1+\frac{\alpha}{\mu}\right)\exp\left[-\frac{\gamma}{\mu}\left(1+\frac{\alpha+\zeta/\gamma}{\mu}\right)t\right]. \tag{3.10}$$

Then, by differentiating (3.10), we obtain

$$\dot{C}(t) \approx -\frac{d}{\beta}\gamma\left(1+\frac{2\alpha+\zeta/\gamma}{\mu}\right)\exp\left[-\frac{\gamma}{\mu}\left(1+\frac{\alpha+\zeta/\gamma}{\mu}\right)t\right]. \tag{3.11}$$

By using (3.10) and (3.11), we can obtain the following estimates of γ_1, γ_2, γ_3, and γ_4:

$$\gamma_1 \approx \gamma_3 \approx \gamma_4 \approx \gamma\left(1+\frac{\alpha+\zeta/\gamma}{\mu}\right), \tag{3.12a}$$

$$\gamma_2 \approx \gamma\left(1+\frac{2\alpha+\zeta/\gamma}{\mu}\right). \tag{3.12b}$$

3.3. Linear approximation of $C(t)$. As mentioned above, the time interval where the exponentially decaying behavior with the first-order-corrected prefactor and decay rate occurs is not clearly defined. We investigate this issue by analyzing the lowest-order terms in $C(t)$ with respect to μ which contribute a linear approximation of $C(t)$ with respect to t.

From (2.17) and (2.25) or alternatively from (2.11) and (2.20), we obtain the following series:

$$C(t) \approx \frac{d}{\beta}\mu\left[1-\frac{1}{\mu}\int_0^t G_0(u)\,du - \frac{1}{\mu^2}\int_0^t G_1(u)\,du + \frac{1}{\mu^2}\int_0^t G_0 * G_0(u)\,du\right]. \tag{3.13}$$

The validity of the above approximation is guaranteed if the higher-order terms are negligible compared with these lowest-order terms. By a rough estimate, the condition is given as $\frac{\gamma}{\mu}t \ll 1$, so by increasing μ, we have a longer time interval.

By using (3.3) and the t-asymptotic expressions

$$\int_0^t G_1(u)\,du = \zeta t + \text{const} \quad \text{for } t > \tau_1, \tag{3.14a}$$

$$\int_0^t G_0 * G_0(u)\,du = \frac{1}{2}\gamma^2 t^2 - 2\alpha\gamma t + \text{const} \quad \text{for } t > 2\tau_0, \tag{3.14b}$$

we obtain, for $t > \max\{2\tau_0, \tau_1\}$,

$$C(t) \approx \frac{d}{\beta}\mu\left(1+\frac{\alpha}{\mu}\right)\left[1-\frac{\gamma}{\mu}\left(1+\frac{\alpha+\zeta/\gamma}{\mu}\right)t\right]. \tag{3.15}$$

Since the validity of (3.13) is guaranteed under the condition $\frac{\gamma}{\mu}t \ll 1$, we collected only constant terms and linear terms in t and neglected γ^2t^2/μ^2. Then we kept only up to the first-order correction terms for the constant terms. Equation (3.15) is the correction to $C(t) \approx C(0)\exp\left(-\frac{\gamma}{\mu}t\right) \approx C(0)\left[1-\frac{\gamma}{\mu}t\right]$ and the estimate of γ_1 is retrieved from it. It is also noted that we have confirmed that this estimate is valid *at least* in the time interval $\max\{2\tau_0, \tau_1\} < t \ll \frac{\mu}{\gamma}$.

3.4. Linear approximation of $\dot{C}(t)$. Similarly, we obtain the expansion

$$\dot{C}(t) = -\frac{d}{\beta}\left[G_0(t) + \frac{1}{\mu}G_1(t) - \frac{1}{\mu}G_0^{*2}(t) + \frac{1}{\mu^2}G_2(t) - \frac{2}{\mu^2}G_0 * G_1(t) + \frac{1}{\mu^2}G_0^{*3}(t)\right], \tag{3.16}$$

where we introduced the second-order correction $G_2(t)$ of $G(t)$ by employing the second-order correction $K_2(t)$ of $K(t)$ and assuming the existence of τ_2. By using the relations

$$G_0 * G_0(t) = \gamma^2 t - 2\alpha\gamma \quad \text{for } t > 2\tau_0, \tag{3.17a}$$

$$G_0 * G_1(t) = \gamma\zeta t + \text{const} \quad \text{for } t > \tau_0 + \tau_1, \tag{3.17b}$$

$$G_0 * G_0 * G_0(t) = \frac{1}{2}\gamma^3 t^2 - 3\alpha\gamma^2 t + \text{const} \quad \text{for } t > 3\tau_0, \tag{3.17c}$$

we obtain, for $t > \max\{3\tau_0, \tau_0 + \tau_1, \tau_2\}$,

$$\dot{C}(t) = -\frac{d}{\beta}\gamma\left(1 + \frac{2\alpha + \zeta/\gamma}{\mu}\right)\left[1 - \frac{\gamma}{\mu}\left(1 + \frac{\alpha + \zeta/\gamma}{\mu}\right)t\right], \tag{3.18}$$

and hence we retrieve the estimates for γ_2 and γ_3 given in (3.12). We note that although we introduced the second-order correction $G_2(t)$, we neglected its contribution, which is a second-order correction to the constant term.

3.5. Linear approximation of $-\dot{C}(t)/C(t)$. By using (3.15) and (3.18), we obtain the following linear approximation of the instantaneous exponential decay rate of $C(t)$:

$$-\frac{\dot{C}(t)}{C(t)} = \frac{\gamma}{\mu}\left(1 + \frac{\alpha + \zeta/\gamma}{\mu}\right), \tag{3.19}$$

which is valid for $\max\{3\tau_0, \tau_0 + \tau_1, \tau_2\} < t \ll \frac{\mu}{\gamma}$. Hence, we retrieve the estimate for γ_4. We note that the slope (with respect to time t) is zero in this first-order correction with respect to μ (i.e., the slope is $o(\mu^{-2})$).

We also derive the limit of the instantaneous exponential decay rate normalized by μ. From (3.13) and (3.16), we obtain

$$-\mu\frac{\dot{C}(t)}{C(t)} \approx G_0(t) + \frac{1}{\mu}G_1(t) + \frac{1}{\mu}\int_0^t G_0(u)\left[G_0(t) - G_0(t-u)\right] du. \tag{3.20}$$

Since $G_1(t)$ and the integral in (3.20) are bounded, we obtain

$$\lim_{\mu\to\infty}\left[-\mu\frac{\dot{C}(t)}{C(t)}\right] = G_0(t). \tag{3.21}$$

We note that the time interval where the approximation (3.20) is valid becomes larger as $\mu \to \infty$ and thus the relation (3.21) is valid for all t.

4. MD simulation results. To confirm the theoretical predictions obtained in sections 2 and 3, we perform MD simulations of the Rayleigh gas system. Although the theoretical predictions obtained for Case A are valid for an interacting bath as well as for an noninteracting bath, we choose this system for the following reasons. First of all, $K_0(t)$ and γ can be accurately obtained from numerical integration of one-particle trajectories of a bath particle for this system [11]. Also, when a purely repulsive interaction potential between the Brownian particle and a bath particle is chosen, $K_0(t)$ and $K_1(t)$ satisfy the assumption on the existence of time scales τ_0 and τ_1, and hence we can verify the results in section 3. On the other hand, when an interaction potential contains an attractive component, these time scales become much longer and may not be clearly defined [11]. By comparing with the results in the purely repulsive potential case, we can observe how the failure of the time scale assumption, which may also occur for Brownian motion in an interacting bath, affects the behavior of the time correlation functions.

Three sets of MD simulations are performed. The first two sets correspond to Case A with a purely repulsive interaction potential and an interaction potential with an attractive component, respectively. The last set is the frozen dynamics simulations corresponding to Case B.

4.1. MD setup. We perform two-dimensional microcanonical-ensemble (NVE) MD simulations. The Weeks–Chandler–Andersen (WCA) potential and the truncated Lennard-Jones (LJ) potential with cutoff 2.5σ are chosen as a purely repulsive interaction potential and an interaction potential containing an attractive component, respectively. The truncated LJ potential $V(r)$ with cutoff r_{cut} is defined as

$$V(r) = \begin{cases} V_0(r) - V_0(r_{\mathrm{cut}}) & \text{if } r < r_{\mathrm{cut}}, \\ 0 & \text{otherwise}, \end{cases} \tag{4.1}$$

where r is the interparticle distance between the Brownian particle and a bath particle and $V_0(r)$ is the LJ potential with parameters ϵ and σ, defined as

$$V_0(r) = 4\epsilon \left[\left(\frac{\sigma}{r}\right)^{12} - \left(\frac{\sigma}{r}\right)^{6} \right]. \tag{4.2}$$

The WCA potential is defined as the truncated LJ potential with cutoff $2^{1/6}\sigma$, where the minimum of $V_0(r)$ is attained. We choose σ as the radius $R = 1$ of the Brownian particle and $\epsilon = 1$.

The system parameters are chosen as follows. For the first two sets of MD simulations, various values of the mass M of the Brownian particle are used: $M = 2$, 5, 10, 20, 50, 100. The mass m of a bath particle is set as $m = 1$, and the number of bath particles is $N = 10^4$. The simulation box is a square with side $L = 100$, and periodic boundary conditions are imposed. The inverse temperature of the system is set as $\beta = 1$. For the last set of MD simulations, the WCA potential is used. Various values of the side of the simulation box are used: $L = 10$, 15, 20, 30, 50, 70, 100. The number of bath particles is correspondingly increased so that the number density is equal to $N/L^2 = 1$. The other parameters are the same except that the mass of the Brownian particle is not defined (i.e., infinite) in this case. All simulation results are reported in reduced units with ϵ the unit of energy, σ the unit of length, and m the unit of mass.

The MD simulations are performed as follows. For the first two sets of MD simulations, the initial position of the Brownian particle is randomly chosen with a uniform distribution in the simulation box, and then the initial positions of the bath particles are randomly chosen with a uniform distribution outside the interaction range of the Brownian particle. The initial velocity of the Brownian particle is set as zero, whereas the velocities of the bath particles are sampled from the Maxwell–Boltzmann distribution. The velocity Verlet algorithm is used for time integration,

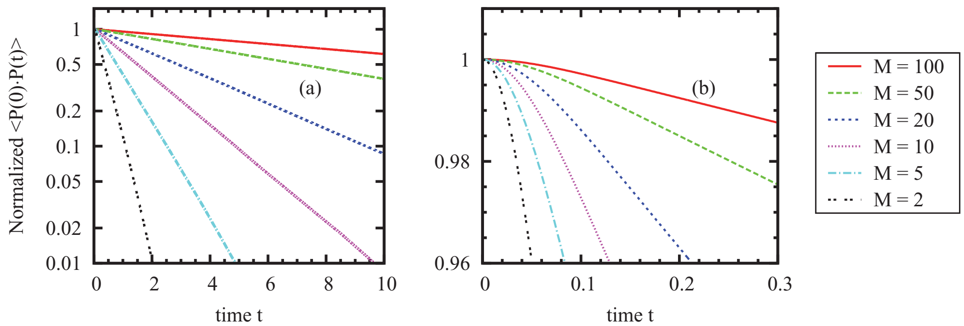

FIG. 1. *For Case A with the WCA potential, the normalized momentum autocorrelation function* $C(t)/C(0)$ *is plotted for various values of the mass* M *of the Brownian particle for long times in panel* (a) *and for short times in panel* (b). *Note that the vertical axis in panel* (a) *is logarithmic scale.*

and the time step size is set as $\Delta t = 10^{-3}$. To obtain a sample in equilibrium, temperature scaling is performed ten times every 10^6 time steps. Then the trajectory is obtained for 5×10^6 time steps for the WCA potential case and for 10^7 time steps for the LJ potential to calculate $\langle \mathbf{P}(0) \cdot \mathbf{P}(t) \rangle$, $\langle \mathbf{P}(0) \cdot \mathbf{F}(t) \rangle$, and $\langle \mathbf{F}(0) \cdot \mathbf{F}(t) \rangle$. For the last set of MD simulations, all procedures are the same except that the Brownian particle is fixed at the randomly chosen initial position and the momentum of the Brownian particle is defined as the negative of the total bath momentum [5].

A total of 128 samples are obtained for each set of the simulation parameters. When a certain physical quantity, for example, $K(t)$, is calculated from the time correlation functions, the statistical error present in the quantity is estimated as follows. The samples are grouped into $n = 8$ bins and the time correlation functions are obtained by averaging over each bin. Using these averaged time correlation functions, 8 samples of the physical quantity are obtained and the sample variance s^2 is calculated. Then the standard deviation of the quantity obtained from the fully averaged time correlation functions over all of the samples is estimated by $\sigma = s/\sqrt{n}$. Owing to a large number of samples, the limiting behavior of the time correlation functions is clearly observed without any significant interference with statistical errors. However, when the first-order corrections for the limiting behavior are investigated, the statistical errors are no longer negligible. In these cases, the error bars corresponding to 3σ are also plotted.

4.2. Case A with WCA potential. We first observe the behavior of the time correlation functions for various values of the mass M of the Brownian particle. Then we confirm the estimates (3.12) of γ_1, γ_2, γ_3, and γ_4 from the time correlation functions after we discuss the behavior of the Mori memory function $K(t)$. Figure 1 shows the time profiles of $C(t) = \langle \mathbf{P}(0) \cdot \mathbf{P}(t) \rangle$ for various values of M. As expected from (1.1a), $C(t)$ decays exponentially at large times, and the exponential decay rate is inversely proportional to the reduced mass μ. However, from the short-time behavior of $C(t)$ it is observed that the slope at $t = 0$ is zero, and it takes some time for $C(t)$ to exhibit a linear decay. The initial zero slope is expected from the fact that $C(t)$ is an even function (i.e., $C(t) = C(-t)$) or from a short-time expansion $C(t) = C(0)\left[1 - \frac{1}{2!}\omega_v^{(2)} t^2 + \frac{1}{4!}\omega_v^{(4)} t^4 \pm \cdots\right]$, where $\omega_v^{(n)}$ is the nth frequency moment [2]. The time profiles of $\dot{C}(t) = \langle \mathbf{P}(0) \cdot \mathbf{F}(t) \rangle$ are shown in Figure 2. As expected from (1.1b),

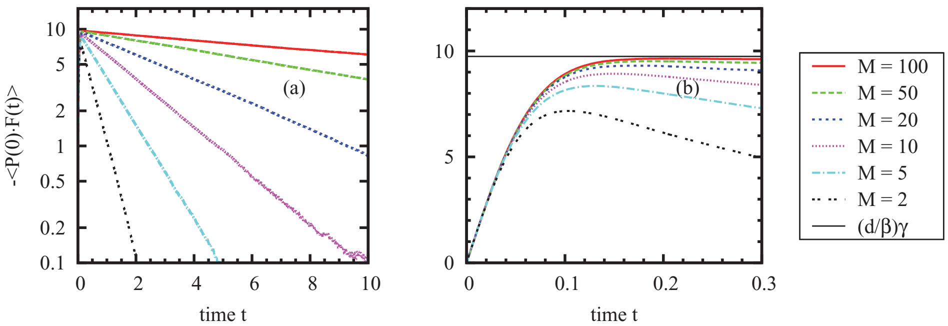

FIG. 2. *For Case A with the WCA potential, the negative of the momentum-force correlation function,* $-\langle \mathbf{P}(0)\cdot\mathbf{F}(t)\rangle = -\dot{C}(t)$*, is plotted for various values of the mass* M *of the Brownian particle for long times in panel* (a) *and for short times in panel* (b)*. The black solid lines indicate the plateau value* $\frac{d}{\beta}\gamma$*. Note that the vertical axis in panel* (a) *is logarithmic scale.*

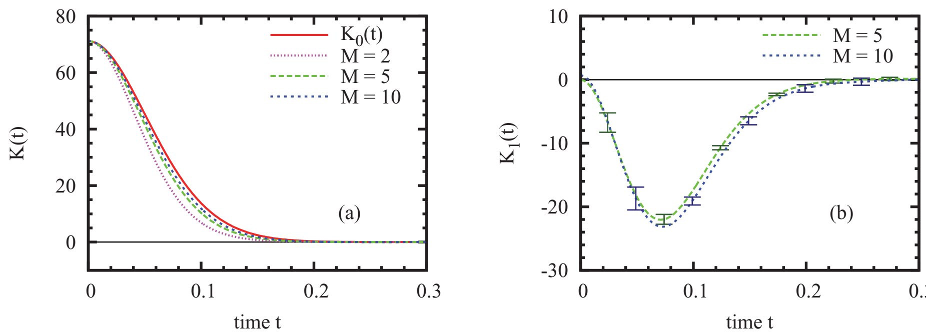

FIG. 3. *For Case A with the WCA potential, the Mori memory function* $K(t)$ *is plotted for various values of the mass* M *of the Brownian particle in panel* (a)*. The limit* $K_0(t) = \lim_{\mu\to\infty} K(t)$ *is also plotted. In panel* (b)*, the time profile of* $K_1(t)$*, which is obtained by subtracting* $K_0(t)$ *from* $K(t)$ *for* $M = 5$ *or* 10 *and multiplying by the corresponding value of* μ*, is plotted with the error bars corresponding to* 3σ*.*

$\dot{C}(t)$ exhibits an exponential decay, at large times, with the same exponential decay rate as $C(t)$. From the short-time behavior of $\dot{C}(t)$ it is observed that the magnitude of $\dot{C}(t)$ is initially zero and, after attaining the maximum, it exhibits a linear decay. As M becomes larger, the maximum approaches the *theoretical plateau* value $\frac{d}{\beta}\gamma = -\lim_{t\to\infty}\lim_{\mu\to\infty}\dot{C}(t)$.

We observe the Mori memory function $K(t)$ in Figure 3. It is calculated from the time correlation functions following the procedure presented in [30]. Its limit under the Brownian limit, $K_0(t) = \lim_{\mu\to\infty} K(t)$, is obtained by numerical integration of one-particle trajectories of a bath particle following the procedure presented in [11]. In the left panel of Figure 3, the time profiles of $K(t)$ for various values of M as well as that of $K_0(t)$ are shown. The convergence of $K(t)$ to $K_0(t)$ is clearly observed as M increases. The next-order correction $K_1(t)$, defined in (2.20), is obtained by using $K(t)$ for intermediate values of M and calculating $\mu\,[K(t) - K_0(t)]$. The time profiles of $K_1(t)$, obtained from the results for $M = 5$ and 10, are shown in the right panel of Figure 3, which show close agreement with each other. As expected from the fact that the initial value $K(0)$ is equal to $\langle \mathbf{F}\cdot\mathbf{F}\rangle$ regardless of the value of M, the initial value

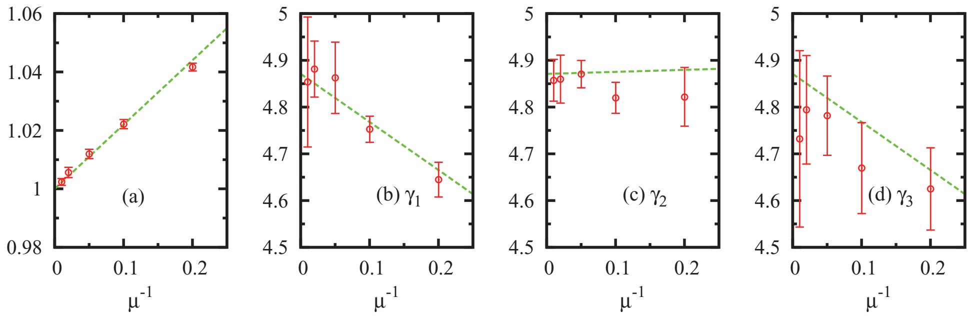

FIG. 4. *For Case A with the WCA potential, the prefactor of the exponential decay of the normalized momentum autocorrelation function at large times is plotted versus the reciprocal of the reduced mass μ in panel* (a). *The values of γ_1, γ_2, and γ_3 are plotted versus μ^{-1} in panels* (b), (c), *and* (d), *respectively. All values are obtained from the linear regression of* $\log(C(t)/C(0))$ *or* $\log|\dot{C}(t)|$. *For details, see the text. The error bars corresponding to 3σ are also plotted. The dotted line in each panel is the theoretical prediction: for* (a), $1+\alpha/\mu$ *and for* (b), (c), *and* (d), *see* (3.12).

of $K_1(t)$ is shown to be zero. The time profile of $K_1(t)$ attains a negative peak and then decays to zero. From the time profiles of $K_0(t)$ and $K_1(t)$, we estimate the time scales of τ_0 and τ_1 of $K_0(t)$ and $K_1(t)$ as 0.2 and 0.3, respectively. The parameters defined in (3.2) are evaluated as $\gamma = 4.87$, $\alpha = 0.22$, and $\zeta = -2.1$.

Using the estimated values of γ, α, and ζ, we confirm the estimates of γ_1, γ_2, γ_3, and γ_4 given in (3.12). For the log plot of the normalized momentum autocorrelation function $C(t)/C(0)$ versus t, linear regression is performed and the slope and intercept are obtained. The time interval for the linear regression is chosen such that the lower endpoint is set as $\tau_0 + \tau_1 = 0.5$ and the upper endpoint is chosen as the time when $C(t)$ decays to one half of the initial value. For $M = 100$, the half-life is longer than $t = 10$ and time interval $[0.5, 10]$ is used instead. The prefactor of the exponential decay of $C(t)/C(0)$ at large times is estimated from the intercept and plotted versus μ^{-1} in panel (a) of Figure 4. The dependence of the prefactor on μ is explained very well by $1+\alpha/\mu$, which is obtained from (3.10). From the slope of the linear regression, the value of γ_1 is estimated by using (3.10) and plotted in panel (b) of Figure 4. As predicted by (3.12), it is observed that as M increases, the value of γ_1 converges to the value of γ and the deviation is proportional to μ^{-1}. For the momentum-force correlation function $\dot{C}(t) = \langle \mathbf{P}(0) \cdot \mathbf{F}(t) \rangle$, linear regression is performed to its log plot using the same time interval as the normalized momentum autocorrelation function. Using (3.11), the values of γ_2 and γ_3 are estimated from the intercept and slope of the linear regression and plotted in panels (c) and (d) of Figure 4, respectively. Their asymptotic behavior is well explained by (3.12). Although the values 2α and ζ/γ, which appears in the estimate of γ_2, happen to cancel each other so we cannot accurately estimate the value $2\alpha+\zeta/\gamma$, it is clearly seen that the slope of the deviation $(\gamma_2 - \gamma)$ with respect to μ^{-1} is different from that of γ_1 and γ_3.

Next, we compile the instantaneous exponential decay rate $-\dot{C}(t)/C(t)$. In the left panel of Figure 5, its time profiles for various values of M are plotted. The instantaneous exponential decay rate attains a plateau after some time which corresponds to $\tau_0 = 0.2$. As M increases, the plateau value, which is normalized by factor μ, increases and approaches to the value of γ. Using the same time interval as the above cases, an extrapolated value at $t = 0$ is obtained from linear regression for each value

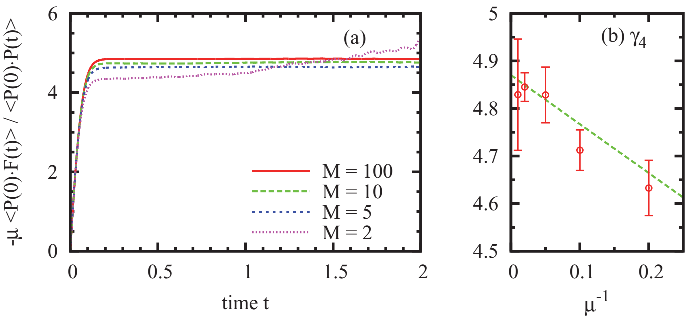

FIG. 5. *For Case A with the WCA potential, the instantaneous exponential decay rate* $-\dot{C}(t)/C(t)$ *normalized by the reduced mass* μ *is plotted, in panel* (a)*, for various values of the mass* M *of the Brownian particle. The plateau values in panel* (a)*, which correspond to* γ_4*, are plotted, with the error bars corresponding to* 3σ*, versus the values of* μ^{-1} *in panel* (b)*. The dotted green line in panel rm(b) indicates the prediction of* (3.12).

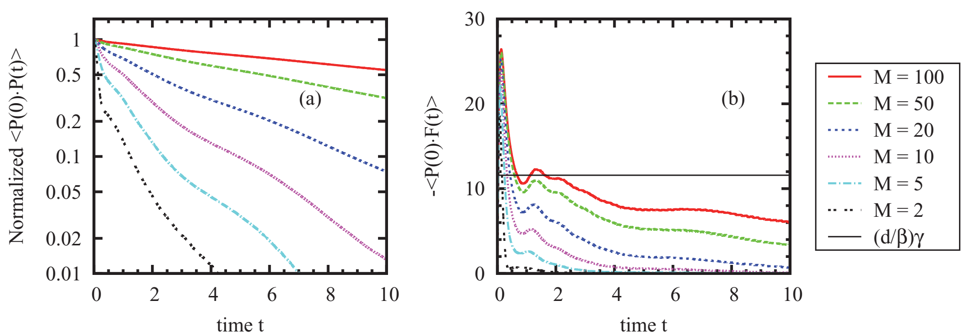

FIG. 6. *For Case A with the LJ potential, the normalized momentum autocorrelation function* $C(t)/C(0)$ *and the negative of the momentum-force correlation function,* $-\dot{C}(t)$*, are plotted in panels* (a) *and* (b)*, respectively, for various values of the mass* M *of the Brownian particle. The plateau value* $\frac{d}{\beta}\gamma$ *is also plotted as a black solid line in panel* (b)*. Note that the vertical axis in panel* (a) *is logarithmic scale.*

of M. It is noted that for linear regression, we use $-\dot{C}(t)/C(t)$ itself rather than its logarithm in this case. In the right panel of Figure 5, these extrapolated values, which correspond to γ_4, are plotted versus μ^{-1}. The convergence of γ_4 to γ is well explained by (3.12). It is also clearly seen that the asymptotic behavior of γ_4 is very similar to those of γ_1 and γ_3.

4.3. Case A with LJ potential. We first compare the decay behavior of the time correlation functions in the LJ potential case with that of the WCA potential case. In Figure 6, the normalized momentum autocorrelation function and the momentum-force correlation functions are shown for various values of M. Although the decay rate decreases as M increases in both correlation functions, the decay is far from being a pure exponential decay. This implies that $K(t)$ has a tail and the microscopic structure of $K(t)$ affects the time correlation functions even at large times.

In Figure 7, the time profiles of $K(t)$ are shown for various of values of M, as well as $K_0(t)$ and $K_1(t)$. Convergence of $K(t)$ to $K_0(t)$ is clearly observed for increasing values of M, and the time profiles of $K_1(t)$ obtained from the results for $M = 5$ and

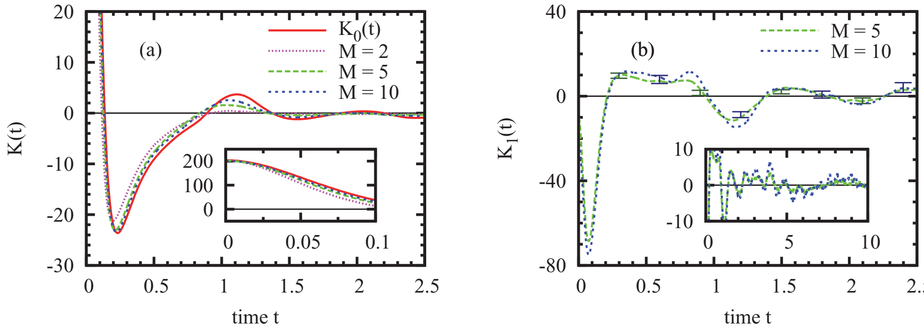

FIG. 7. *For Case A with the LJ potential, the time profiles of the Mori memory function $K(t)$ are plotted for various values of the mass M of the Brownian particle in panel* (a). *The limit $K_0(t) = \lim_{\mu\to\infty} K(t)$ is also plotted. In the inset, the main peak of $K(t)$ at short times is plotted. In panel* (b), *the time profiles of $K_1(t)$, which are obtained by using the results of $M = 5$ and $M = 10$, are plotted with the error bars corresponding to 3σ. In the inset, the tails of $K_1(t)$ are plotted.*

10 agree very well with each other, which confirms our assumption on the asymptotic form of $K(t)$, (2.20). However, the time scales τ_0 and τ_1 cannot be clearly defined in this case; $K_0(t)$ has an oscillating tail due to the effect of the trapped bath particles to the potential well of the LJ potential [11], and it is observed that $K_1(t)$ also has an oscillating tail.

Since both the exponential decay and the influence of the microscopic structure affect the time correlation functions over the whole time interval of our observation, we fail to accurately estimate the values of γ_1, γ_2, and γ_3. These values vary for different choices of the time interval for the curve fitting since the time correlation functions do not exhibit a pure exponential decay. However, for γ_4, it is expected that the effect of the exponential decay disappears or is reduced significantly since the exponential decay of $C(t)$ and $\dot{C}(t)$ may cancel in the instantaneous exponential decay rate, $-\dot{C}(t)/C(t)$. In Figure 8, the instantaneous exponential decay rate is plotted for various values of M. It does not exhibit an exponential decay, and at large times it starts to form a plateau. For $M = 100$, the instantaneous exponential decay rate is calculated up to $t = 20$, and it is confirmed that it attains a plateau. In addition, as predicted from (3.20) and (3.21), it is observed that for each t, $-\dot{C}(t)/C(t)$ approaches $G_0(t)$, which is the time integral of $K_0(t)$, as M increases. The deviation is inversely proportional to the reduced mass μ.

4.4. Case B. We first observe a characteristic behavior of $\dot{C}(t)$ in the frozen dynamics of the Rayleigh gas system. Figure 9 shows the time profiles of $-\dot{C}(t)$ for various values of the simulation box size L. We use the values of $\dot{C}(t)$ obtained from the time integral of the force autocorrelation function rather than those obtained from the momentum-force correlation function since the latter contain much larger statistical errors than the former. This is because the momentum of the Brownian particle is defined as the negative of the total momentum of the bath particles, and thus its variance is very large in this case. Contrary to Case A, we observe that $\dot{C}(t)$ attains a plateau before it starts to decay. For $L = 10$, 15, and 20, the duration of exhibiting such a plateau is proportional to L and the plateau value becomes closer to the value of γ as the system size increases. The deviation of the plateau value from γ is observed to be inversely proportional to L^2. It is also observed that even after

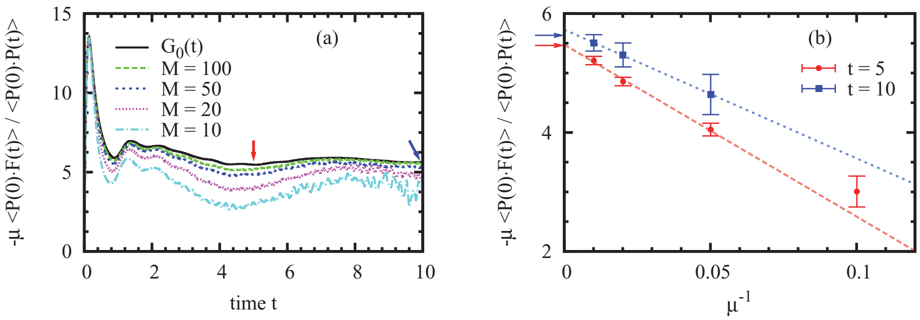

FIG. 8. *For Case A with the LJ potential, the instantaneous exponential decay rate $-\dot{C}(t)/C(t)$ normalized by factor μ is plotted for various values of the mass M of the Brownian particle in panel* (a)*. The time integral of $K_0(t)$, i.e., $G_0(t)$, is also plotted. As M increases, the deviation of $-\mu\dot{C}(t)/C(t)$ from $G_0(t)$ is observed to decrease like* $\mathrm{O}(\mu^{-1})$ *for all points on the time axis. Two time points $t = 5$ and $t = 10$, representative of the cases $t < \tau_0$ and $t \approx \tau_0$, are chosen and their values $-\mu\dot{C}(t)/C(t)$ versus μ^{-1} are plotted with corresponding linear regressions in panel* (b)*. To reduce statistical errors, the time-averaged values of $-\mu\dot{C}(t)/C(t)$ over short time intervals* [5,5.1] *and* [9.9,10] *are used. The error bars correspond to 3σ. The square for $t = 10$ and $M = 10$ is omitted since the value is not reliable due to large decay of $C(t)$ and $\dot{C}(t)$. The arrows in panel* (a) *indicate the location of the time points ($t = 5$ for the left arrow and $t = 10$ for the right one) where two sets of data in panel* (b) *are obtained, whereas the arrows at the vertical axis in panel* (b) *indicate the corresponding values of $G_0(t)$ ($t = 5$ for the bottom arrow and $t = 10$ for the top one).*

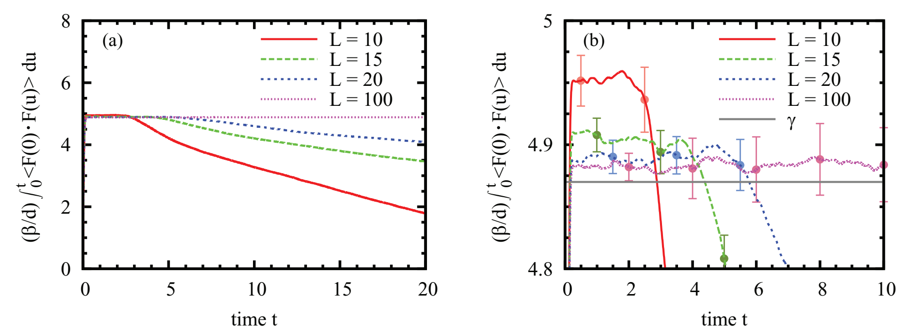

FIG. 9. *For Case B (with the WCA potential), $-\dot{C}(t)$ evaluated from the time integral of the force autocorrelation function is plotted for various values of the box size L in panel* (a)*. In panel* (b)*, the same quantity is plotted near the value of γ, which is plotted as a dotted line. It is noted that the error bars corresponding to σ rather than 3σ are plotted for clear presentation.*

the plateau region, $\dot{C}(t)$ does not exhibit a clear exponential decay.

As mentioned in section 2.5.2, this characteristic behavior of $\dot{C}(t)$ is explained by the tail of the force autocorrelation function which develops in the finite-size Rayleigh gas system. In the left panel of Figure 10, the time profiles of the force autocorrelation function for $L = 10$, 15, and 20 are compared by using scaled time t/L and scaling factor L^2. The scaled tails show good agreement with each other, which confirms (2.29). In the right panel of Figure 10, the Mori memory function is compared with the force autocorrelation function for $L = 10$. The overall shape of $K(t)$ is similar to $\langle \mathbf{F}(0) \cdot \mathbf{F}(t) \rangle$ and is lifted by $-\frac{\beta}{d\mu} K_0 * \dot{C}_0(t)$ as predicted from (2.31).

For larger values of L, the decay is not observed and the momentum-force correlation function maintains the plateau up to $t = 10$, which is the maximum time of

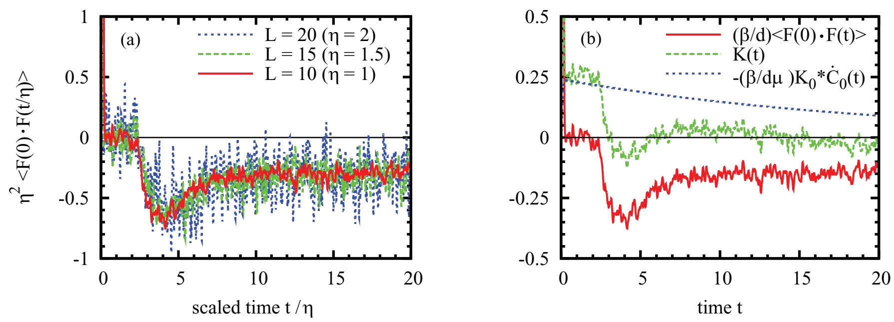

FIG. 10. *For Case B, the time profiles of the force autocorrelation function for various values of the box size* L *are plotted in panel* (a). *Following* (2.29)*, scaled time* t/η *and scaling factor* η^2 *are used. In panel* (b)*, the tails of the force autocorrelation and the Mori memory function for* $L = 10$ *are compared. The time profile of* $K_0 * \dot{C}_0(t)$ *is also plotted.*

our observation. In this case, the momentum autocorrelation function exhibits a pure exponential decay.

5. Summary and discussion. For a Brownian particle suspended in a bath, corrections to the (t,μ)-asymptotic expressions of $\langle \mathbf{P}(0) \cdot \mathbf{P}(t) \rangle$ and $\langle \mathbf{P}(0) \cdot \mathbf{F}(t) \rangle$, (1.1a) and (1.1b), have been obtained in (3.10) and (3.11). Using these corrections, it has been shown that various numerical methods which estimate the value of the friction coefficient γ using the exponential decay of the time correlation functions at large times produce $\gamma + O(\mu^{-1})$; see (3.12).

To obtain these results, the asymptotic expansion of $C(t) = \langle \mathbf{P}(0) \cdot \mathbf{P}(t) \rangle$, (2.24), has been derived by solving the Volterra integrodifferential equation (2.8) and by introducing the asymptotic expansion of the Mori memory function $K(t)$. The lowest-order term $C_0(t)$ in the asymptotic expansion of $C(t)$ is defined in terms of the Mori memory function $K_0(t)$ of the infinite reference system. $C_0(t)$ itself is given as a series of convolution powers, and higher-order terms in the asymptotic expansion of $C(t)$ are given as multiple convolutions of $C_0(t)$ with higher-order terms in the asymptotic expansion of $K(t)$.

By introducing time scales τ_0 and τ_1 of $K_0(t)$ and $K_1(t)$, (t,μ)-asymptotic expressions of $C_0(t)$ and $C(t)$, (3.8) and (3.10), have been derived. However, owing to a feature of convolution, each term in the asymptotic expansion of $C_0(t)$ and $C(t)$ has different length of transient time before it exhibits a t-asymptotic behavior, and hence the time intervals, where the asymptotic expressions are valid, become questionable. To address this issue, lower-order terms in the asymptotic expansions of $C(t)$ and $\dot{C}(t)$ have been analyzed and the validity time intervals for the *linear* decay expressions, (3.15) and (3.18), have been found. The lower endpoint of the time intervals is determined by τ_0 and τ_1, whereas the upper endpoint is given by the condition $\frac{\gamma}{\mu} t \ll 1$. However, it is noted that our result does not imply that the *exponential* decay behavior is only valid in these intervals. Our analysis demonstrates one of the essential reasons that the evaluation of the friction coefficient is not straightforward; there are two limits involved (i.e., the Brownian limit and the long time limit), and they are not interchangeable with each other. Since it is virtually impossible to simulate the infinite reference system using the MD simulation technique, (2.16) cannot be used as it is from MD simulations. Instead, a finite system corresponding to a large value of μ is simulated and a long-time behavior in a certain time interval is observed. As shown in our analysis, an appropriate choice of the time interval depends on not only the microscopic times t_0 and t_1 but also the condition determined by the value of μ.

For a Rayleigh gas under the WCA potential, which satisfies the time scale assumption, the theoretical predictions have been confirmed by a systematic MD simulation study. In particular, as predicted from (3.12), γ_2 has been shown to have a different first-order correction from those of γ_1, γ_3, and γ_4. Then, to observe a case where the assumption of the time scales fails, a counterpart system under the LJ potential has been investigated. Due to the influence of the oscillating tail, it has been observed that the decay is not clearly exponential even at large times, and accurate evaluation of γ_1, γ_2, and γ_3 fails. However, the normalized instantaneous exponential decay rate defined as $-\mu\dot{C}(t)/C(t)$ has been observed to have the following favorable features that make γ_4 a practically better measure of γ than γ_1, γ_2, and γ_3: first, the quantity does not exhibit an exponential decay and eventually forms a plateau; second, it is easily calculated from the time correlation functions; third, for each t, it converges to the time integral of the Mori memory function up to time t as $\mu \to \infty$; see (3.20) and (3.21).

Our approach is new in the sense that the Mori memory function is employed and explicit dependence of the time correlation functions in the near-Brownian-limit regime on the memory function is determined. A close connection of the Mori memory function to the Brownian motion theory has been pointed out from several points of view [5, 10, 15]. Compared with Mazur and Oppenheim's memory function, Mori's memory function $K(t)$ can be relatively easily calculated from the time correlation functions. However, since its analytic properties are not so favorable as those of the former [10], determining an asymptotic expansion of $K(t)$ may not be straightforward, and some physical arguments or numerical experiments are needed. For the infinite mass limit (i.e., Case A), by previous theoretical analysis [10, 23], a simple form, (2.20), has been found. As a *counter*example, we have considered the frozen dynamics of the Rayleigh gas in a finite bath. We have demonstrated that due to the boundary conditions $\dot{C}(t)$ exhibits a characteristic behavior, which is not explained by the asymptotic expression of $C_0(t)$, and $K(t)$ has a different form from Case A. Considering that several MD simulation studies have performed frozen dynamics simulations and determined the value of γ by using (1.1), a future investigation on asymptotic behavior of the time correlation functions along the thermodynamic limit is called for.

In this paper, we have analyzed one of the prototypical systems where multiscales are present and play an important role. Our work has provided a method of evaluating the friction coefficient γ in a systematic manner. A precise evaluation of γ is essential for mesoscopic simulation methods such as Langevin/Brownian dynamics and dissipative particle dynamics. Since the time scale of the Brownian motion is not completely separated from that of the surrounding fluid particles in the phenomena simulated by these methods, consideration of the asymptotic behavior of the time correlation function of the Brownian particle at microscopic times will help to develop a more realistic model.

Appendix. The scaling property of the tail present in the force autocorrelation function due to the re-collisions of bath particles to the periodic images of the Brownian particle is derived for a finite-volume Rayleigh gas under periodic boundary conditions, where the fixed Brownian particle interacts with the gas through elastic collisions. By considering a bath particle colliding with the Brownian particle and subsequently with its periodic image, we calculate the autocorrelation function of the force exerted on the Brownian particle or its image by the bath particle. The scaling

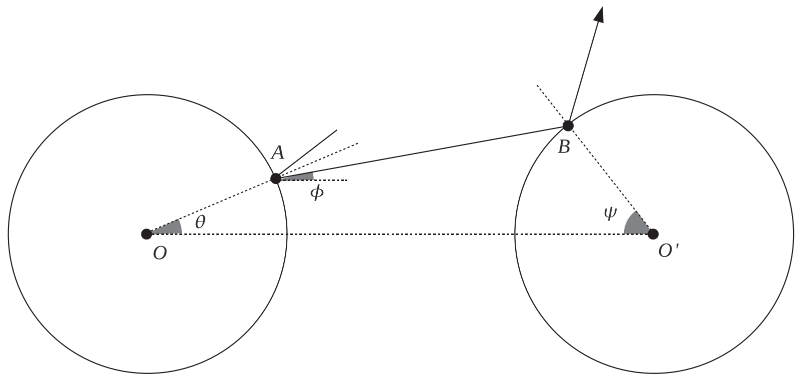

FIG. 11. *A typical trajectory of a bath particle sequentially colliding with the fixed Brownian particle at the origin O and its image at O'. The Brownian particle and its image are represented as disks of radius R and the bath particle elastically collides at points A and B. The angles $\angle AOO'$ and $\angle BO'O$ and the angle between $\overline{AB}$ and the horizontal line are denoted as θ, ψ, and ϕ, respectively. While θ and ϕ are counterclockwise angles from the horizontal lines, ψ is a clockwise angle. It is assumed that the separation L between the Brownian particle and its image is much larger than R.*

parameter is the separation distance L between the Brownian particle and its image, which is assumed to be much larger than the radius R of the Brownian particle. We first consider the two-dimensional case and then discuss the general case.

For simplicity, we assume that there is a single image. We denote the positions of the Brownian particle and its image by $O(0,0)$ and $O'(L,0)$, respectively. By introducing θ and ψ, we denote the points at which the bath particle collides with the Brownian particle and its image as $A(R\cos\theta, R\sin\theta)$ and $B(L-R\cos\psi, R\sin\psi)$, respectively (see Figure 11). We also denote the angle formed by the line $\overline{AB}$ and the horizontal line as ϕ and its possible range as $\phi_1 < \phi < \phi_2$. Since $\lim_{L\to\infty} L\phi_1 = -R(1+\sin\theta)$ and $\lim_{L\to\infty} L\phi_2 = R(1-\sin\theta)$, we have $\phi = \mathrm{O}(L^{-1})$. By denoting the magnitude of the bath particle's velocity as v and the time duration that it moves from A to B as t_{AB}, vt_{AB} satisfies $(R\cos\theta + vt_{AB}\cos\phi - L)^2 + (R\sin\theta + vt_{AB}\sin\theta)^2 = R^2$. Since $vt_{AB} = L + \delta x$ with $\delta x = \mathrm{O}(1)$ for large L, we obtain $\delta x = -R\cos\theta - \sqrt{R^2 - (R\sin\theta + L\phi)^2} + \mathrm{O}(L^{-1})$. Hence, we obtain an expression for ψ in terms of θ and ϕ: $\sin\psi = \sin\theta + \frac{L\phi}{R} + \mathrm{O}(L^{-1})$.

The impulses exerted on the bath particle during the collisions at A and B are expressed as $\mathbf{I}_A = 2mv\cos(\theta-\phi)(\cos\theta, \sin\theta)$ and $\mathbf{I}_B = 2mv\cos(\psi+\phi)(-\cos\psi, \sin\psi)$, respectively. By denoting the time when the bath particle collides at A by t_A, the force it exerts on the Brownian particle or its image is expressed as $\mathbf{F}(t) = -\mathbf{I}_A\delta(t-t_A) - \mathbf{I}_B\delta(t-t_A-t_{AB})$. Hence, we have $\langle \mathbf{F}(0)\cdot\mathbf{F}(t)\rangle = \left\langle |\mathbf{I}_A|^2\delta(-t_A)\delta(t-t_A)\right\rangle + \langle \mathbf{I}_A\cdot\mathbf{I}_B\delta(-t_A)\delta(t-t_A-t_{AB})\rangle \equiv c_1(t) + c_2(t)$. The first term $c_1(t)$ corresponds to the result for the infinite reference system (i.e., without the image of the Brownian particle), whereas the second term $c_2(t)$ is the contribution of the re-collision to the image. Following a similar procedure demonstrated in [11], the ensemble averages $c_1(t)$ and $c_2(t)$ are obtained by averaging with respect to the equilibrium distribution of the initial condition of the bath particle. We denote the initial position and velocity as $(r\cos\chi, r\sin\chi)$ and $(v\cos\omega, v\sin\omega)$, respectively, and assume that the equilibrium measure is approximated by that of the infinite reference system (i.e., $(a\mathbb{I}_{\{r\geq R\}}rdrd\chi)(\frac{m\beta}{2\pi}e^{-\frac{1}{2}\beta mv^2}vdvd\omega)$, with a the number density of bath particles), which becomes valid for $r \ll L$ and $R \ll L$. By using that $\delta(t_A) =$

$v|\cos(\chi-\omega)|\delta(r-R)$ for $\frac{1}{2}\pi+\chi<\omega<\frac{3}{2}\pi+\chi$, we perform integration with respect to r and consider $r\to R+$ for the remaining integration with respect to χ, ω, and v. By symmetry, we only need to consider the case $0<\chi<\frac{\pi}{2}$ and multiply by factors 4 and 2 for $c_1(t)$ and $c_2(t)$, respectively. We have $\theta\to\chi$ and $\phi\to 2\chi-\omega-\pi$ as $r\to R+$. Through the integration

$$\text{(A.1)}\quad 4m^2aR\left(\int_0^\infty \frac{m\beta}{2\pi}v^4e^{-\frac{1}{2}\beta mv^2}dv\right)\left(4\int_0^{\frac{\pi}{2}}d\chi\int_{\chi+\frac{1}{2}\pi}^{\chi+\frac{3}{2}\pi}|\cos(\chi-\omega)|^3d\omega\right)\delta(t),$$

we obtain $c_1(t)=\frac{8aR}{\beta}\sqrt{\frac{2\pi m}{\beta}}\delta(t)$, which leads to the friction coefficient $\gamma=2aR\sqrt{\frac{2\pi m}{\beta}}$ for the infinite reference system [11].

In order to estimate $c_2(t)$, we note that the interval of ω for the re-collision is of length $\mathrm{O}(L^{-1})$ from the constraint $\phi_1<\phi<\phi_2$. Since $\omega\in(2\chi-\pi-\frac{R}{L}(1-\sin\chi),2\chi-\pi+\frac{R}{L}(1+\sin\chi))$, we approximate the integrand by its value at $\omega_0=2\chi-\pi$ and consider the width of the interval $\Delta w=\frac{2R}{L}$. We note that ω_0 corresponds to the case that the trajectory of the bath particle from A to B is parallel to the horizontal line. Then $\mathbf{I}_A\cdot\mathbf{I}_B$ is approximated by $-4m^2v^2\cos^2\chi\cos 2\chi$, whereas $\delta(t_A)$ is by $v\cos\chi\delta(r-R)$. On the other hand, since $t_A\to 0$ as $r\to R+$, $\delta(t-t_A-t_{AB})$ can be replaced by $\delta(t-t_{AB})$ in the integrand, which is further approximated by $\delta(t-\frac{L}{v})=\frac{L}{t^2}\delta(v-\frac{L}{t})$. Hence, through the integration

$$\text{(A.2)}\quad -4m^2aR\left(\frac{L}{t^2}\int_0^\infty \frac{m\beta}{2\pi}v^4e^{-\frac{1}{2}\beta mv^2}\delta\left(v-\frac{L}{t}dv\right)\right)\left(2\Delta w\int_0^{\frac{\pi}{2}}\cos^3\chi\cos 2\chi d\chi\right),$$

we finally obtain

$$\text{(A.3)}\qquad c_2(t)\approx -\frac{16aR^2m^3\beta}{5\pi L^2}\left(\frac{L}{t}\right)^6 e^{-\frac{1}{2}m\beta\left(\frac{L}{t}\right)^2}.$$

Hence, $c_2(t)$ has a form of $L^{-2}f\left(\frac{t}{L}\right)$.

For the three-dimensional case, the integration with respect to two spherical angles for the initial velocity gives $\mathrm{O}(L^{-2})$ dependence. This is because in order for the bath particle to collide with the image, both angles should be in narrow intervals of length $\mathrm{O}(L^{-1})$. The integration with respect to the magnitude v of the bath particle's velocity gives the same form of the L-dependence as in the two-dimensional case. That is, integrating $g(v)\delta(t-t_A-t_{AB})$ with respect to v gives $\frac{L}{t^2}g(\frac{L}{t})$. Hence, we obtain $L^{-3}f(\frac{t}{L})$. We can generalize this result for the d-dimensional case and conclude that $c_2(t)$ has a form of $L^{-d}f(\frac{t}{L})$.

Acknowledgment. Computations were performed at the IBM BG/P and BG/Q with computer time provided by an INCITE grant.

REFERENCES

[1] M. Bologna, *Asymptotic solution for first and second order linear Volterra integro-differential equations with convolution kernels*, J. Phys. A, 43 (2010), 375203.
[2] J. P. Boon and S. Yip, *Molecular Hydrodynamics*, Dover, New York, 1991.
[3] D. Dürr, S. Goldstein, and J. L. Lebowitz, *A mechanical model of Brownian motion*, Comm. Math. Phys., 78 (1981), pp. 507–530.
[4] P. S. Epstein, *On the resistance experienced by spheres in their motion through gases*, Phys. Rev., 23 (1924), pp. 710–733.

[5] P. Español and I. Zúñiga, *Force autocorrelation function in Brownian motion theory*, J. Chem. Phys., 98 (1993), pp. 574–580.
[6] M. S. Green, *Brownian motion in a gas of noninteracting molecules*, J. Chem. Phys., 19 (1951), pp. 1036–1046.
[7] E. H. Hauge and A. Martine-Liöf, *Fluctuating hydrodynamics and Brownian motion*, J. Statist. Phys., 7 (1973), pp. 259–281.
[8] E. J. Hinch, *Application of the Langevin equation to fluid suspensions*, J. Fluid Mech., 72 (1975), pp. 499–511.
[9] R. Huang, I. Chavez, K. M. Taute, B. Lukić, S. Jeney, M. G. Raizen, and E.-L. Florin, *Direct observation of the full transition from ballistic to diffusive Brownian motion in a liquid*, Nature Phys., 7 (2011), pp. 576–580.
[10] J. T. Hynes, R. Kapral, and M. Weinberg, *Microscopic theory of Brownian motion: Mori friction kernel and Langevin equation derivation*, Physica, 80A (1975), pp. 105–127.
[11] C. Kim and G. E. Karniadakis, *Microscopic theory of Brownian motion revisited: The Rayleigh model*, Phys. Rev. E, 87 (2013), 032129.
[12] J. G. Kirkwood, *The statistical mechanical theory of transport processes*, J. Chem. Phys., 14 (1946), pp. 180–201.
[13] G. R. Kneller and K. Hinsen, *Computing memory functions from molecular dynamics simulations*, J. Chem. Phys., 115 (2001), pp. 11097–11105.
[14] G. R. Kneller, K. Hinsen, and G. Sutmann, *Mass and size effects on the memory function of tracer particles*, J. Chem. Phys., 118 (2003), pp. 5283–5286.
[15] G. R. Kneller and G. Sutmann, *Scaling of the memory function and Brownian motion*, J. Chem. Phys., 120 (2004), pp. 1667–1669.
[16] S. Kusuoka and S. Liang, *A classical mechanical model of Brownian motion with plural particles*, Rev. Math. Phys., 22 (2010), pp. 733–838.
[17] J. L. Lebowitz and E. Rubin, *Dynamical study of Brownian motion*, Phys. Rev., 131 (1963), pp. 2381–2396.
[18] S. H. Lee and R. Kapral, *Friction and diffusion of a Brownian particle in a mesoscopic solvent*, J. Chem. Phys., 121 (2004), pp. 11163–11169.
[19] D. S. Lemons and A. Gythiel, *Paul Langevin's 1908 paper "On the Theory of Brownian Motion" ["Sur la théorie du mouvement brownien," C. R. Acad. Sci. (Paris) 146, 530–533 (1908)]*, Amer. J. Phys., 65 (1997), pp. 1079–1081.
[20] T. Li, S. Kheifets, D. Medellin, and M. G. Raizen, *Measurement of the instantaneous velocity of a Brownian particle*, Science, 328 (2010), pp. 1673–1675.
[21] V. Lisý, J. Tóthová, and L. Glod, *On the correlation properties of thermal noise in fluids*, Int. J. Thermophys., 34 (2013), pp. 629–641.
[22] R. M. Mazo, *Momentum-correlation function in a Rayleigh gas*, J. Chem. Phys., 35 (1961), pp. 831–835.
[23] P. Mazur and I. Oppenheim, *Molecular theory of Brownian motion*, Physica, 50 (1970), pp. 241–258.
[24] D. Montgomery, *Brownian motion from Boltzmann's equation*, Phys. Fluids, 14 (1971), pp. 2088–2090.
[25] H. Mori, *Transport, collective motion, and Brownian motion*, Progr. Theoret. Phys., 33 (1965), pp. 423–455.
[26] F. Ould-Kaddour and D. Levesque, *Determination of the friction coefficient of a Brownian particle by molecular-dynamics simulation*, J. Chem. Phys., 118 (2003), pp. 7888–7891.
[27] J. Petravic, *Equilibrium calculation of the friction coefficient for a massive particle moving in finite liquid volume*, J. Chem. Phys., 129 (2008), 114502.
[28] J. Petravic, *Force autocorrelation in linear response theory and the origin of friction*, J. Chem. Phys., 129 (2008), 094503.
[29] P. Résibios and H. T. Davis, *Transport equation of a Brownian particle in an external field*, Physica, 30 (1964), pp. 1077–1091.
[30] H. K. Shin, C. Kim, P. Talkner, and E. K. Lee, *Brownian motion from molecular dynamics*, Chem. Phys., 375 (2010), pp. 316–326.
[31] G. Sutmann and B. Steffen, *Correction of finite size effects in molecular dynamics applied to the friction coefficient of a Brownian particle*, Comput. Phys. Comm., 147 (2002), pp. 374–377.
[32] R. Zwanzig, *Elementary derivation of time-correlation formulas for transport coefficients*, J. Chem. Phys., 40 (1964), pp. 2527–2533.
[33] R. Zwanzig and M. Bixon, *Compressibility effects in the hydrodynamic theory of Brownian motion*, J. Fluid Mech., 69 (1975), pp. 21–25.